Single-Turnover Kinetics of Homoprotocatechuate 2,3-Dioxygenase†

Stephanie L. Groce, Marcia A. Miller-Rodeberg,‡ and John D. Lipscomb*

Department of Biochemistry, Molecular Biology, and Biophysics and Center for Metals in Biocatalysis, University of Minnesota, Minneapolis, Minnesota 55455

Received June 23, 2004; Revised Manuscript Received September 21, 2004

ABSTRACT: Homoprotocatechuate 2,3-dioxygenase isolated from *Brevibacterium fuscum* utilizes an active site Fe(II) and O_2 to catalyze proximal extradiol cleavage of the substrate aromatic ring. In contrast to other members of the ring cleaving dioxygenase family, the transient kinetics of the extradiol dioxygenase catalytic cycle have been difficult to study because the iron is nearly colorless and EPR silent. Here, it is shown that the reaction cycle kinetics can be monitored by utilizing the alternative substrate 4-nitrocatechol (4NC), which is also cleaved in the proximal extradiol position. Changes in the optical spectrum of 4NC occurring as a result of ionization, environmental changes, and ring cleavage allow both the substrate binding and product formation phases of the reaction to be studied. It is shown that substrate binding occurs in a four-step process probably involving binding to two ionization states of the enzyme at different rates. Following an initial rapid binding of the monoanionic 4NC in the active site, slower binding to the Fe(II) and conversion to the dianionic form occur. The bound dianionic 4NC reacts rapidly with O_2 in four additional steps, apparently occurring in sequence. On the basis of the optical properties of the intermediates, these steps are hypothesized to be O_2 binding to the iron, isomerization of the resulting complex, ring opening, and product release. The natural substrate appears to form the same intermediates but with much larger rate constants. These are the first transient intermediates to be reported for an extradiol dioxygenase reaction.

Extradiol aromatic ring-cleaving dioxygenases allow the aerobic bacterial utilization and/or degradation of a vast array of aromatic compounds of both natural and man-made origin in the environment (*1*−*4*). One such enzyme is homoprotocatechuate 2,3-dioxygenase isolated from *Brevibacterium fuscum* (2,3-HPCD)[1] that catalyzes the Fe(II)-dependent oxidative cleavage of 3,4-dihydroxyphenylacetate (HPCA) to yield α-hydroxy *δ*-carboxymethyl *cis*-muconic semialdehyde as illustrated below (*5*).

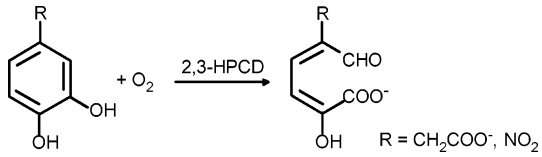

2,3-HPCD is a member of the type I extradiol dioxygenase subfamily which includes the archetypal catechol 2,3-dioxygenase (2,3-CTD) and the biphenyl 1,2-dioxygenases, DHBD and BphC (*4*). Each of these enzymes requires active site Fe(II) for activity. An isoform of 2,3-HPCD, MndD from *Arthrobacter globiformis*, is very similar in amino acid sequence and structure, but requires active site manganese for activity (*6*). The X-ray crystal structures of these dioxygenases have been determined (*7*−*10*) and reveal that the active site metal is ligated by two histidines, one glutamate residue, and two or three solvents, placing them in the so-called 2-His-1-carboxylate facial triad superfamily (*11*). The active site structures of 2,3-HPCD and its anaerobic HPCA complex are shown in Scheme 1.

Mechanistic studies of extradiol dioxygenases have been slowed by the fact that the Fe(II) center is nearly colorless and EPR silent. In past studies, we have circumvented these problems to some extent through the use of NO as a probe for O_2 binding in the active site (*2*, *5*, *12*). The NO complex of the active site iron exhibits an intense $S = {}^3/_2$ EPR signal that is sensitive to the presence of substrate. It was shown that substrate-free extradiol dioxygenases do not bind O_2 and only weakly bind NO (*13*). When added, substrate forms a chelate complex with the iron via its two hydroxyl groups, and this causes NO to bind much more strongly in another

† This work was supported by National Institutes of Health Grant GM24689 (J.D.L.). S.L.G. was supported in part by NIH Training Grant GM008347.

* To whom correspondence should be addressed: Department of Biochemistry, Molecular Biology, and Biophysics, University of Minnesota, 6-155 Jackson Hall, 321 Church St. SE, Minneapolis, MN 55455. E-mail: lipsc001@umn.edu. Telephone: (612) 625-6454. Fax: (612) 624-5121.

‡ Current address: Department of Chemistry, University of Wisconsin, 105 Garfield Ave., Eau Claire, WI 54702.

[1] Abbreviations: 4NC, 4-nitrocatechol; HPCA, homoprotocatechuate or 3,4-dihydroxyphenylacetate; PCA, protocatechuate; MOPS, 3-morpholinopropanesulfonic acid; 2,3-HPCD, homoprotocatechuate 2,3-dioxygenase from *Brevibacterium fuscum*; MndD, homoprotocatechuate 2,3-dioxygenase from *Arthrobacter globiformis*; 3,4-PCD, protocatechuate 3,4-dioxygenase; 2,3-CTD, catechol 2,3-dioxygenase; DHBD, dihydroxybiphenyl 1,2-dioxygenase from *Burkholderia* sp. LB400; BphC, dihydroxybiphenyl 1,2-dioxygenase from *Pseudomonas* sp. KKS102; E, E′, E−4NC(1), E′−4NC(1), E−4NC(2), E−4NC(3), and E−4NC(4), enzyme intermediates formed during binding of 4NC to 2,3-HPCD; E−4NC−O_2(1), E−4NC−O_2(2), and E−4NC−O_2(3), enzyme intermediates formed during the oxygen binding and product forming segment of the 2,3-HPCD turnover reaction with 4NC.

10.1021/bi048690x CCC: $27.50
Published on Web 11/10/2004

Scheme 1: Active Site Iron (cyan) Ligation of 2,3-HPCD (top) and Its Anaerobic HPCA Complex (bottom)[a]

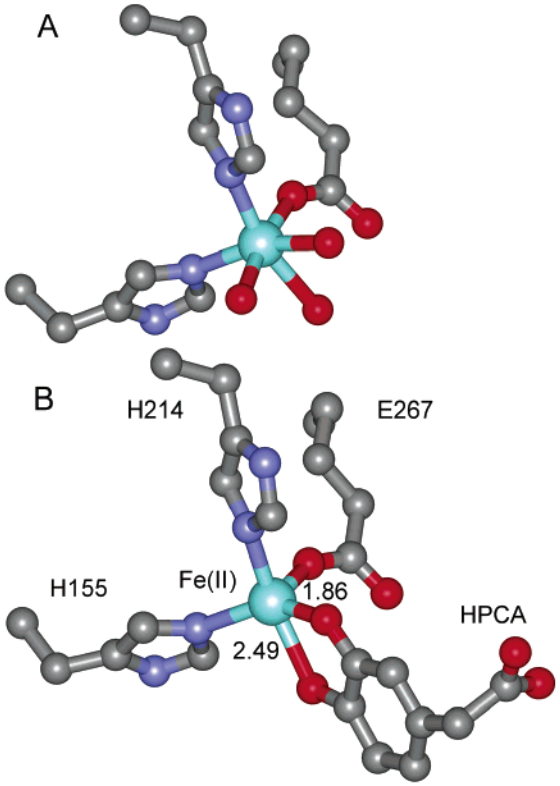

[a] Note the asymmetric binding of substrate to the iron that is thought to be due to ionization of the C3-OH group but not of the C4-OH group of bound HPCD (distances in angstroms). Structures are from ref *10*. PDB entries 1F1X (top) and 1Q0C (bottom).

coordination site of the iron. Thus, three sites in the iron coordination sphere are available for exogenous ligands to promote the reaction chemistry. It was proposed that, by analogy, substrate binding may also greatly increase the affinity of the enzyme for O_2, thereby providing a mechanism for ordering the reaction and ensuring that substrate is present when O_2 is activated.

Other types of spectroscopies, including XANES, EXAFS, Mössbauer, MCD/CD, and UV-resonance Raman (*12*, *14*−*17*), have also been used to study the extradiol dioxygenases and their substrate complexes. These studies indicate that the substrate binds as a chelated monoanion, displacing the solvent ligands from the iron. Because there is only one endogenous anionic ligand in the iron coordination sphere (Glu267 in the case of 2,3-HPCD), and it is likely that only one of the liganding solvents is ionized, this binding mode would maintain a charge-neutral metal center often found in non-heme oxygenase enzymes (*18*, *19*). The recent X-ray crystal structures (e.g., Scheme 1) confirm all of these findings and indicate that the open coordination site where O_2 or NO might bind is next to the vicinal substrate coordination sites. This binding site was later confirmed by the solution of the structure of the NO−BphC−substrate complex (*20*).

On the basis of this organization of the active site, we and others have proposed that the Fe(II) plays a number of roles in catalysis, some of which are illustrated in Scheme 2 (see Scheme 7 for more detail) (*2*, *3*, *9*, *13*, *16*, *20*−*22*). The direct coordination of both the organic substrate and

Scheme 2: Some Key Steps in the Proposed Reaction Mechanism of Extradiol Dioxygenases (*14*, *21*)

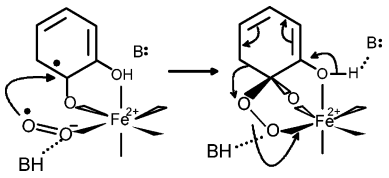

O_2 to the Fe(II) would allow their relative orientations to be controlled, and it would also permit transfer of electron density between them. The reaction is hypothesized to begin by substrate binding to the iron, resulting in the release of the solvent ligands and transfer of electron density from the ligand to the metal to promote O_2 binding. Delocalization of electron density onto the O_2 would result in a nascent superoxide that might then attack the adjacent, partially electron deficient, aromatic substrate to form an initial peroxy adduct. A Criegee rearrangement (*23*) would result in cleavage of the O−O bond and insertion of one atom of oxygen into the substrate aromatic ring adjacent to the vicinal hydroxyl functions with retention of the second oxygen atom on the metal at the level of water. Attack on the resulting lactone by the metal-bound oxygen would result in ring opening to form the product. Finally, product release with return of solvents to the coordination sphere would complete the reaction cycle.

This proposal for the reaction cycle implies many intermediates that might be sufficiently stable to detect. In related studies of intradiol-cleaving catecholic dioxygenases and *cis*-diol-forming Rieske type dioxygenases, it proved to be possible to detect intermediates in the reaction cycles due to the presence of relatively intense endogenous chromophores that change in absorbance during catalysis (*24*−*29*). In the case of the extradiol dioxygenases, this has not been possible because the spectroscopic techniques described above that are amenable for the study of the Fe(II) center are not as well suited to time-resolved measurements on the millisecond scale.

In this study, a new approach is described in which the reaction cycle of 2,3-HPCD is monitored via changes in a chromophoric substrate and products rather than direct observation of the metal center. Past studies showed that, unlike most other aromatic ring-cleaving dioxygenases, 2,3-CTD (*30*), 2,3-HPCD (*5*), and MndD (*31*) catalyze oxidative ring opening of 4-nitrocatechol (4NC) in the proximal extradiol position, which is analogous to the ring opening position for HPCA. However, in contrast to HPCA, 4NC exhibits a chromophore in the visible region that changes dramatically with the ionization state and environment of its two hydroxyl functions (*30*). Also, the ring cleavage products of both HPCA and 4NC turnover are intensely yellow. Each of these chromophores can be used to monitor and quantitate the complete single-turnover reaction of 2,3-HPCD. It is shown here for the first time that intermediates can be detected in the catalytic cycle of an extradiol dioxygenase. These intermediates expand our view of the active site chemistry of this important enzyme class.

EXPERIMENTAL PROCEDURES

Reagents. All chemicals were purchased from Sigma-Aldrich and were used without purification except for HPCA,

PCA, and 4NC which were recrystallized at 4 °C to remove minor contaminants. 3,4-PCD was purified as previously described (*32*). Anaerobic conditions were achieved by repeated cycling of solutions between argon gas and vacuum. Trace contaminating O_2 was removed from the Ar gas by passing it over a BASF copper catalyst at 150 °C.

Overexpression of 2,3-HPCD in Escherichia coli and Purification. 2,3-HPCD was overexpressed in *E. coli* strain BL21-(DE3) and subsequently purified as previously described (*33*).

Enzyme and Metal Quantification. The concentration of purified 2,3-HPCD was routinely determined using the absorbance at 280 nm ($\epsilon = 1.14$ mg^{-1} cm^{-1}). The optical absorption was measured using a Hewlett-Packard 8453 spectrophotometer. Metal was quantified using a Varian SpectrAA-100 flame atomic absorption spectrometer at 248.3 nm.

Steady-State Kinetic Measurements. 2,3-HPCD was assayed for dioxygenase activity using two methods. In the first method, the rate of O_2 consumption was monitored by using a Clark-type oxygen electrode as previously described (*32*) using 3,4-PCD and PCA for standardization. In the second method, the rate of product formation was directly monitored optically. At pH 7.5, the proximal cleavage product of HPCA has a maximum absorption at 380 nm (ϵ_{380} = 36 000 M^{-1} cm^{-1}). 4NC turnover activity was measured at pH 7.5 at 330 nm using a $\Delta\epsilon_{330}$ of 12 060 M^{-1} cm^{-1}, which is the difference extinction coefficient for 4NC (1840 M^{-1} cm^{-1}) and the product (13 900 M^{-1} cm^{-1}). Standard assay conditions were 22 °C, 50 mM MOPS, and pH 7.5, although determinations were also made at 4 °C for comparison with the transient kinetic results. Initial velocity data were analyzed as a hyperbolic function of substrate concentration to determine K_m and V_{max} using KFIT, a nonlinear regression program by N. C. Millar (King's College, London, U.K.).

Determination of the Dissociation Constant for 4NC. The K_d for 4NC was determined by titration into an enzyme solution in 50 mM MOPS buffer (pH 7.5) in an anaerobic cuvette at 22 °C. The E−4NC complex was quantified at 600 nm (ϵ = 3.2 mM^{-1} cm^{-1}) where only the dianionic form of 4NC contributes significantly. The bound dianionic 4NC was subtracted from the total 4NC added to determine the unbound concentration. The data, plotted as fraction 4NC bound versus free 4NC, were fit to the hyperbolic eq 1 using KFIT.

$$\text{fraction 4NC bound} = [\text{4NC free}]/(K_d + [\text{4NC free}]) \quad (1)$$

Transient Kinetic Experiments. All experiments, except where noted, were conducted under pseudo-first-order conditions using an Applied Photophysics model SX.18MV stopped flow device at 4 °C. The reactions were monitored either at a selected wavelength or by using a diode array detector to record the entire visible range at each time point. Under these conditions, reaction time courses can be simulated using one or more summed exponential functions. The time courses for single-wavelength data can be fit to eq 2 using nonlinear regression.

$$\text{absorbance}_t = a_0 + \text{Amp}_1\, e^{-t/\tau_1} + \text{Amp}_2\, e^{-t/\tau_2} + \ldots \quad (2)$$

where the amplitude terms are composed of rate constants, wavelength-dependent $\Delta\epsilon$ values, and a normalizing concentration term (generally the total enzyme concentration). The constant a_0 term represents the distribution of species present at the completion of the reaction expressed in absorbance units. The total number of exponential terms and reciprocal relaxation time values ($1/\tau_n$) are equal to the number of steps in the actual reaction as long as no internal cycles occur. The order of the exponential phases is not necessarily the order of the steps in the reaction.

The pseudo-first-order binding kinetics of 4NC were monitored by anaerobically mixing solutions of 20 μM enzyme [Fe(II) sites] with 4NC (5−160-fold excess), where all concentrations are after mixing. The system was initially made anaerobic by flushing the lines with 10 mM dithionite followed by rinsing with anaerobic buffer. All anaerobic transfers were made with gastight Hamilton syringes. The three reciprocal relaxation times derived from the fitting process for this reaction were plotted as a function of 4NC concentration. The plot of $1/\tau_1$ versus 4NC concentration was found to be hyperbolic, which is indicative of a rapid unobserved initial binding step (see the Results). For this type of reaction, the values $k_{forward}$ and $k_{reverse}$ for the observed step and K_d for the unobserved binding step can be determined using eq 3 (*25*).

$$1/\tau_{obs} = (k_{forward}[\text{4NC}])/(K_d + [\text{4NC}]) + k_{reverse} \quad (3)$$

For pH-dependent turnover and transient kinetic studies, measurements were carried out over the pH range of 5.5−10.0. All buffers were prepared at a concentration of 50 mM, and the conductivity of all buffers was adjusted to a constant value with a minimal amount of 3 M NaCl. The measured conductivity of the buffers was 645 ± 12.3 μS/cm. Buffers used were MES (pH 5.5−6.3), MOPS (pH 6.6−7.5), TAPS (pH 7.8−8.7), and CHES (pH 9.0−10.0).

The pseudo-first-order binding kinetics for the reaction between the preformed E−4NC complex and O_2 were monitored by first combining the enzyme and 4NC anaerobically to a final concentration of 100 μM [Fe(II) sites], a value well in excess of the overall K_d for the complex. This mixture was transferred to the stopped-flow instrument in a gastight syringe and mixed rapidly with buffer equilibrated with O_2 at final concentrations of 4−14 times the Fe(II) concentration [the final enzyme concentration was 50 μM Fe(II) sites].

For single-turnover experiments monitoring the complete turnover cycle, enzyme and 4NC were mixed stoichiometrically at 50 μM [Fe(II) sites after mixing] in air-saturated 50 mM MOPS (pH 7.5). Progress curves were fit as described in the text.

Simulations of reaction time courses were performed using the numerical integration program KSIM by N. C. Millar. Rate constants and extinction coefficients determined from the reciprocal relaxation times and phase amplitudes were used with various hypothetical reaction schemes to attempt to match the observed time courses.

Chemical Quench Procedures. For both hand and mechanical-mixing chemical quench reactions, 100 μM E−4NC-(3) (see Scheme 3 for nomenclature) in 50 mM MOPS (pH 7.5) was mixed with O_2-saturated buffer. In the case of hand mixing (reaction times of >3 s), 100 μL of 100 μM E−4NC-(3) in a gastight Hamilton syringe was mixed with 100 μL of O_2-saturated buffer in a 0.5 mL reaction vial on ice. After

the prescribed time period (4, 6, 20, and 60 s), the reaction was quenched with 200 μL of 10% metaphosphoric acid. In the case of the mechanically mixed samples for shorter reaction times, the enzyme and O_2 solutions (total of 250 μL) were mixed at 4 °C using an Update Instruments model 1010 rapid mixing instrument and pushed into a delay line. After a prescribed delay of 50−2000 ms, a second push deposited the solution through a spray nozzle into 200 μL of 10% metaphosphoric acid. Samples from both procedures were centrifuged for 1 min at full speed in a microcentrifuge. The supernatant was made basic by the addition of 50 μL of 6 N NaOH and the optical spectrum recorded. While the optical spectrum of 4NC is strongly pH-dependent in the neutral to high pH range, that of the extradiol cleavage product is not. Basic conditions result in an increase in absorption of 4NC at 550 nm while having little effect on the spectrum of the cleavage product, thereby allowing for quantitative analysis based on the extinction coefficients at 550 nm for 4NC (12 510 M^{-1} cm^{-1}), and at 390 nm for 4NC (8740 M^{-1} cm^{-1}) and the product (18 250 M^{-1} cm^{-1}).

Product Identification. The extradiol product of 4NC formed by wild-type 2,3-HPCD was isolated from the reaction mixture by ultrafiltration using YM-30 Centricon devices in a JA-17 rotor at 5000*g* for 30 min at 4 °C, lyophilized, and resuspended in deuterated DMSO for ^{1}H NMR studies. The solvent signal was used as a field-frequency lock and chemical shift reference. All NMR measurements employed a Varian Unity Inova 600 MHz spectrometer.

RESULTS

Optical Spectra of 4NC, Enzyme−4NC Complexes, and the Cleavage Reaction Product. Figure 1 shows the spectra of 4NC in its three ionization states ($pK_{a1} = 6.89$ and $pK_{a2} = 10.75$) (*30*, *34*) and in its anaerobic complex with 2,3-HPCD at pH 7.5. In solution at pH 7.5, 4NC exists in approximately 85% monoanion and 15% fully protonated states. The spectrum of the 2,3-HPCD−4NC complex reveals that the bound 4NC is predominantly in the dianionic form, suggesting a large shift in the apparent ionization constant for at least one hydroxyl group. This provides an optical probe for the reaction that allowed the determination of the K_d for 4NC binding under anaerobic conditions (5 ± 2 μM, Figure 1, inset) as well as the observation of the kinetic time course of the binding process described below.

The 4NC ring cleavage product has an absorption maximum at 390 nm ($\epsilon_{390} = 21\,000$ M^{-1} cm^{-1} at pH 7.5) with a shoulder at 330 nm as shown in Figure 1. The site of ring cleavage was determined to be between ring carbons 2 and 3 (proximal position) by ^{1}H NMR spectroscopy. The NMR spectrum of the product shown in Figure 2 exhibits a sharp singlet at 10.00 ppm, characteristic of aldehydic protons, and two signals that can be assigned to olefinic protons at 7.68 ppm (doublet, $J = 15$ Hz) and 6.96 ppm (doublet, $J = 15$ Hz). The presence of the aldehydic proton is diagnostic of extradiol cleavage, while the fact that it is a singlet demonstrates cleavage in the proximal rather than the distal position. The large shift in the spectrum upon ring cleavage provides an optical probe that was used in the studies described below to observe the time course of the product forming process.

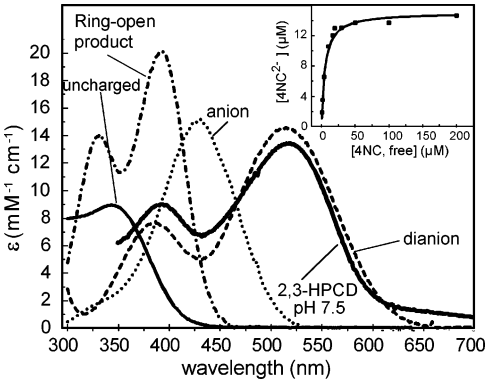

FIGURE 1: UV−visible spectra of 4NC species in solution and bound to 2,3-HPCD. Shown are spectra of 4NC in solution at pH 2 [neutral (—)], pH 7.5 [anion (•••)], and pH 12 [dianion (- - -)] as well as 2,3-HPCD−4NC (thick solid line) and the cleavage product of 4NC (-•-), both at pH 7.5. The inset shows a titration of 2,3-HPCD with 4NC, measured at 600 nm and pH 7.5 (dianion formation). The solid line represents a hyperbolic fit to the data.

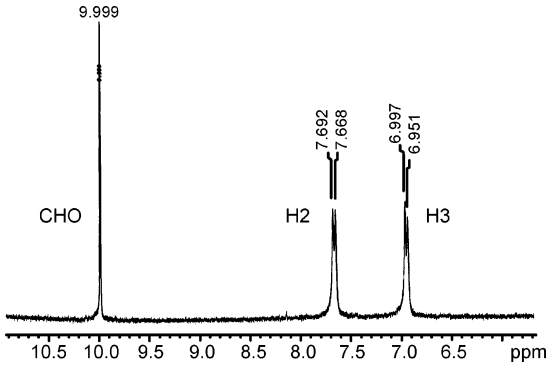

FIGURE 2: ^{1}H NMR spectrum of the product from 4NC ring cleavage. The product was isolated from 2,3-HPCD by ultrafiltration, then lyophilized, and resuspended in DMSO-d_6.

Table 1: Steady-State Kinetic and Thermodynamic Parameters of 2,3-HPCD[a]

parameter	4NC	HPCA
k_{cat} (s^{-1})	0.4	10
k_{cat}(4 °C) (s^{-1})	0.05 ± 0.01	3.2 ± 0.2
K_m (μM)	15	25
pH optimum	6.9	8.4
K_d (μM)	5 ± 2	>2

[a] In 50 mM MOPS buffer at pH 7.5 and 22 °C except where noted. The values were determined as described in Experimental Procedures.

The steady-state kinetic parameters and equilibrium binding data for 4NC and HPCA as substrates for 2,3-HPCD are summarized in Table 1.

Transient Kinetics of the Anaerobic Binding of 4NC to 2,3-HPCD. The kinetics of the first half of the reaction, the binding of 4NC to 2,3-HPCD, were monitored using a UV−vis stopped-flow instrument at 4 °C and pH 7.5. 2,3-HPCD (20 μM iron sites) was mixed anaerobically with 4NC in a 5−160-fold molar excess to satisfy pseudo-first-order conditions. The time course monitored at 512 nm was best fit by a summation of three well-resolved exponential phases, all with positive amplitudes, as shown in Figure 3A and summarized in Table 2. This shows that there are at least three observable steps related to binding.

The 4NC concentration dependence of the observed reciprocal relaxation times gives additional insight into the

Table 2: Reciprocal Relaxation Times and Phase Amplitudes for 2,3-HPCD Reactions[a]

substrate and reaction	phase 1[b] (% total amplitude)	phase 2 (% total amplitude)	phase 3 (% total amplitude)
4NC			
binding	$42 \pm 2\ s^{-1}$ (45.5%[d])	$1.9 \pm 0.1\ s^{-1}$ (4.5%)	$0.15 \pm 0.02\ s^{-1}$ (42.2%)
O_2 reaction[c]	$1.8 \pm 0.1\ s^{-1}$ (−4.6%[e])	$0.31 \pm 0.03\ s^{-1}$ (54.5%)	$0.07 \pm 0.02\ s^{-1}$ (40.9%)
HPCA			
O_2 reaction[c]	$38 \pm 3\ s^{-1}$ (−10%[f])	$3.2 \pm 0.2\ s^{-1}$ (90%)	

[a] Reaction starting conditions and procedures are described in Experimental Procedures and in the text. Buffer: 50 mM MOPS, pH 7.5, 4 °C. [b] Each reaction also includes a fast, unobserved phase that occurs due to binding of either substrate to the enzyme or O_2 to the enzyme−substrate complex in the dead time of the stopped-flow instrument (see the text). [c] Initiated from the preformed stoichiometric enzyme−substrate complex. [d] At 512 nm. [e] At 390 nm. [f] At 380 nm.

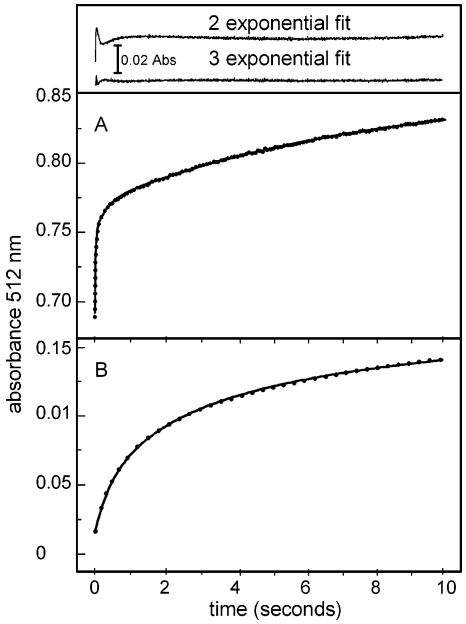

FIGURE 3: Anaerobic binding reaction of 4NC with 2,3-HPCD. (A) 4NC (2.4 mM) was mixed anaerobically in a stopped-flow device with 20 μM 2,3-HPCD (iron sites), and dianion formation was monitored at 512 nm. The progress curve (···) was fit with two or three summed exponential functions, and the residuals of these fits are shown at the top of the plot. The solid line superimposed on the time course represents the three-exponential fit of the data. (B) Reaction of 20 μM 2,3-HPCD (iron sites) and 20 μM 4NC under anaerobic conditions (···). Shown superimposed is a numerical integration simulation of the time course using the model and rate constants shown in Scheme 3B. Extinction coefficients ($mM^{-1}\ cm^{-1}$) used in the simulation were 0.4 for 4NC, 0.4 for E−4NC(1), 0.4 for E′−4NC(1), 13.0 for E−4NC(2), and 13.5 for E−4NC(3). Conditions for both panels A and B: 50 mM MOPS, pH 7.5, and 4 °C.

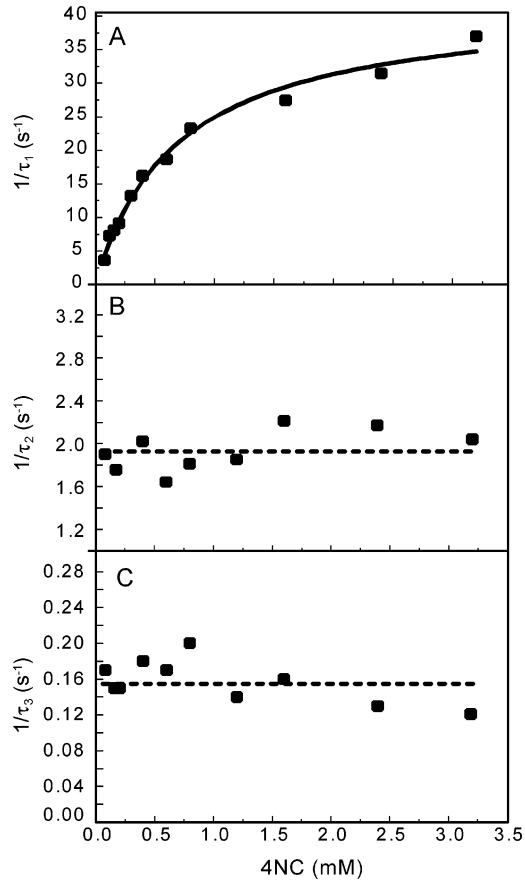

FIGURE 4: Reciprocal relaxation times for the phases in the anaerobic formation of the 2,3-HPCD−4NC complex plotted as a function of 4NC concentration. 2,3-HPCD [20 μM, Fe(II) sites] was reacted anaerobically with varying concentrations of 4NC that ranged from 80 μM to 3.2 mM (all concentrations after mixing) using a stopped-flow device. Conditions: 50 mM MOPS, pH 7.5, and 4 °C.

nature of the reaction. As shown in Figure 4, the two smaller reciprocal relaxation times, $1/\tau_2$ and $1/\tau_3$, are apparently independent of 4NC concentration, so at least one step in the binding reaction must be separated from the initial binding event by a nearly irreversible step. The largest reciprocal relaxation time, $1/\tau_1$, does depend strongly on substrate concentration, but the fact that the plot shown in Figure 4A is nonlinear shows that the reaction being monitored does not reflect the binding event itself. The hyperbolic fit to the observed $1/\tau_1$ plot is expected for a two-step binding process and yields the following constants (see eq 3 in Experimental Procedures): $k_{forward} = 40 \pm 2\ s^{-1}$, $k_{reverse} = 2 \pm 2\ s^{-1}$, and $K_d(4NC) = 325 \pm 25\ \mu M$. The dissociation constant for the formation of the first (unobserved) complex is nearly 2 orders of magnitude larger than that for the static 4NC complex, consistent with the observation of a nearly irreversible second step in the binding process following the initial complex formation. This would also account for the lack of a 4NC concentration dependence for the slower reciprocal relaxation times under the assumption that the binding steps occur in sequence. Thus, the simplest overall binding process is illustrated in Scheme 3A.

The data shown in Figure 3 indicate that the fast, unobserved first step in Scheme 3A occurs with little spectroscopic change because the point observed at 3 ms (twice the dead time) has about the same absorbance as the starting 4NC. This suggests that 4NC remains monoanionic during this fast step. The steps that follow lead to the final dianionic E−4NC complex.

Scheme 3: Two Reaction Scenarios To Account for the Observation of Three Kinetic Phases in the Anaerobic Binding Reaction of 4NC with 2,3-HPCD

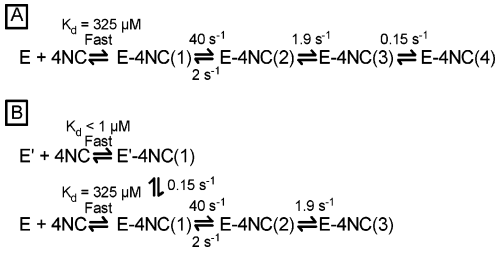

One potential difficulty with Scheme 3A is that the amplitudes of the fastest and slowest observed phases are similar throughout the 4NC concentration range that has been examined and together account for most of the optical change. For a linear series of steps, this would require that there be a substantial change in the extinction coefficient at 512 nm between the E−4NC(2) complex and one of the later species. This seems unlikely given that the only two species that can be monitored are the mono- and dianionic forms of 4NC, so once deprotonation occurs, little further change in extinction is expected. Accordingly, there is a near-isosbestic point at 465 nm suggesting similar extinction coefficients for the later intermediates.

An alternative to Scheme 3A (Scheme 3B) invokes two forms of the enzyme, E and E′, that interconvert very slowly. Both bind 4NC rapidly, but the E′−4NC(1) complex must be nearly irreversibly formed to account for the loss of an apparent concentration dependence in the slower phases. In Scheme 3B, the rate-limiting step in the formation of the final stoichiometric enzyme−substrate complex (sum of forward and reverse rate constants approximately equal to $1/\tau_3$) is the conversion of the E′−4NC(1) complex to the E−4NC(1) complex. Because the substrate free E and E′ forms do not directly interconvert on the time scale of the binding reaction in this model, two of the phase amplitudes would be expected to reflect the relative concentrations of these species and not change substantially as the 4NC concentration is changed, as observed.

Numerical integration simulations over a wide range of initial 4NC concentrations show that either Scheme 3A or Scheme 3B can be used to give a good fit to the data. This is illustrated for the anaerobic reaction of stoichiometric 2,3-HPCD (sites) and 4NC shown in Figure 3B. Under these conditions, exponential fitting is not appropriate. Nevertheless, the rate constants determined by exponential fitting at high 4NC concentrations can still be used to adequately simulate the data. Although both schemes describe the experimental rate constant data equally well, Scheme 3B is preferred on the basis of amplitude analysis. In this scheme, each species can be assigned an extinction coefficient approximately equal to that of either the mono- or dianionic form of 4NC in solution, while Scheme 3A requires an intermediate value for the E−4NC(2) species. Importantly, for Scheme 3B, the same extinction coefficients can be used throughout the entire concentration range that has been examined, whereas new values must be used for each new concentration in the case of Scheme 3A.

The nature of the two forms of the enzyme indicated in Scheme 3B is unknown. However, the ratio of the first to the third phase amplitude increases with an increase in pH,

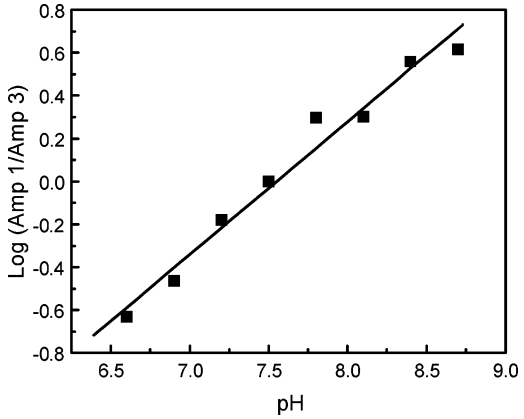

FIGURE 5: pH dependence of the phase amplitude ratio for formation of the E−4NC(2) complex. The anaerobic reaction between 600 μM 4NC and 30 μM 2,3-HPCD (sites, all concentrations after mixing) was monitored and analyzed as described in the legend of Figure 3A. The ratio of the amplitudes of the first and third phases is plotted according to the Henderson−Hasselbach relationship.

suggesting that two different ionization states of the enzyme are involved. The pH dependence shows that the protonated state is less reactive. Thus, under the protein ionization-state hypothesis, the ratio of amplitudes 1 and 3 would approximate the ratio of the ionized to un-ionized species. If ionization is responsible for the effects, then a plot of the log of the amplitude ratio versus pH is expected to be linear, and this is the case as shown in Figure 5 (apparent pK_a = 7.5). However, if a single ionizable group is involved, the slope of the plot should be 1, and it is actually 0.62 ± 0.1. This may be due to the presence of several ionizable groups that contribute to substrate binding, or the model present in Figure 3B may still be too simple; for example, E might actually convert to E′ dynamically during the binding process as E′ is trapped in the E′−4NC(1) form. Nevertheless, it appears that the two forms are likely to be related by the ionization state of an active site base or one of the solvents bound to the Fe(II) rather than a posttranslational modification of the enzyme or another permanent change in the enzyme structure.

The rate of steady-state turnover of 4NC at pH 7.5 and 4 °C is 0.05 ± 0.01 s^{-1}. Thus, none of the rate constants associated with 4NC binding correspond to the rate-limiting step in turnover.

Single Turnover of the Preformed E−4NC Complex. The second half of the single-turnover reaction was studied by first forming the anaerobic, stoichiometric E−4NC complex in one stopped-flow syringe using a concentration (100 μM sites) well above the overall K_d of 5 μM for 4NC binding in 50 mM MOPS (pH 7.5). This was then rapidly mixed with O_2-containing buffer under pseudo-first-order conditions from the second syringe. These conditions permitted only a single turnover beginning from the enzyme−substrate complex [nominally E−4NC(3)].

The time-dependent diode array spectra of the reaction are shown in Figure 6A. The approximate isosbestic point at 440 nm indicates that each species that forms during the course of this reaction has a spectrum similar to those of either the starting 4NC dianion complex or the product. However, careful inspection (see the inset of Figure 6A) shows that spectra early and late in the time course do not pass

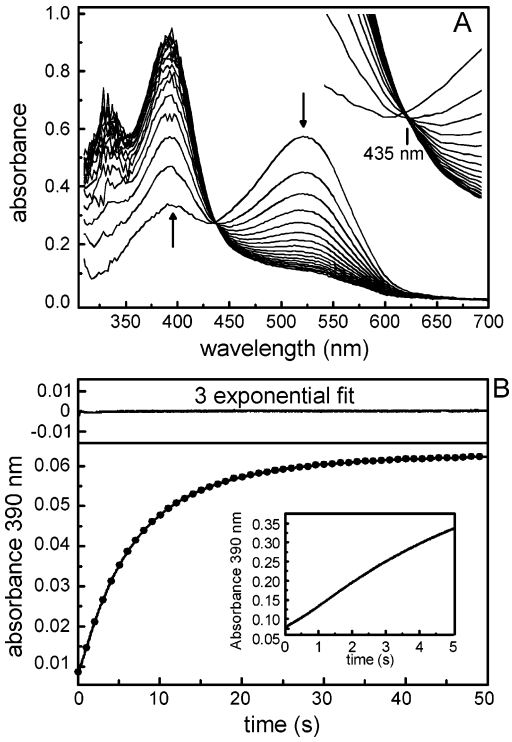

FIGURE 6: Single turnover of the preformed 2,3-HPCD−4NC complex upon exposure to O_2. (A) Diode array spectra taken during the first 65 s of the reaction after mixing 50 μM E−4NC(3) and 210 μM O_2 solution (concentrations after mixing). The inset emphasizes the fact that there is a deviation from the apparent isosbestic point at 435 nm at the beginning and end of the reaction. (B) Single-wavelength time course (···) of the reaction recorded at 390 nm and a superimposed three-exponential fit (—). The residuals are shown above the trace. There is a slight sigmoidicity to the beginning of the time course (inset) that reveals the presence of the third phase. A two-exponential fit also reproduces the experimental data well except during the first 5 s of the reaction where a large deviation between experiment and fit is observed. Conditions: 50 mM MOPS, pH 7.5, and 4 °C.

precisely through the same point showing that discrete intermediates exist. This is demonstrated by the single-wavelength time course data shown in Figure 6B. The time course at 390 nm, where both 4NC dianion and product absorb, exhibits a subtle lag phase (i.e., a phase with a small negative amplitude; see the inset of Figure 6B) in addition to two slower exponential phases with large positive amplitudes. The kinetic parameters for the reaction are listed in Table 2. The smallest reciprocal relaxation time of 0.07 ± 0.02 s^{-1} is equal within error to the steady-state turnover number at 4 °C (0.05 ± 0.01 s^{-1}), suggesting that the rate-limiting step occurs during this part of the overall reaction cycle.

These data indicate that the reaction of the E−4NC complex with O_2 occurs in a multistep process, but do not distinguish whether the steps occur in series or in parallel. Insight into this question might be derived from the O_2 concentration dependence of the reaction, but none of the phases exhibited a dependence at pH 7.5 (data not shown). Unfortunately, the O_2 concentration range that can be used is limited because at high O_2 concentrations a new chromophoric species that is maximized at ~445 nm slowly appears during the reaction. Figure 7 shows the optical spectra of the product formed at low O_2 (210 μM) and high O_2 (700 μM) concentrations. As the O_2 concentration is increased, it is evident that the yield of product decreases

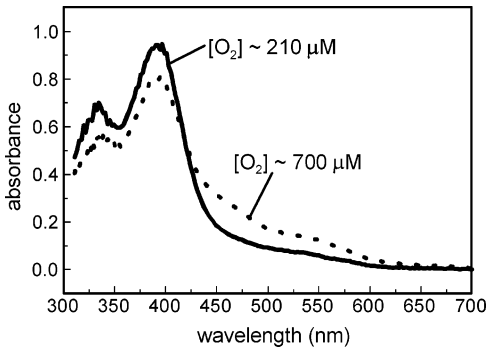

FIGURE 7: Optical spectra showing the effect of varying O_2 concentrations in the single-turnover reaction of the preformed 2,3-HPCD−4NC complex upon exposure to O_2. The reaction was as described in the legend of Figure 6 at low (210 μM) and high (700 μM) O_2 concentrations. The reaction was monitored by rapid scan diode array detection, and the final spectrum after 120 s is shown.

Scheme 4: Proposed Intermediates in the Reaction of the Preformed 2,3-HPCD−4NC Complex with O_2

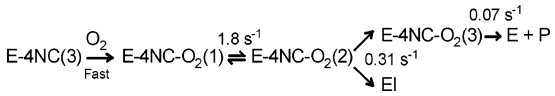

concomitant with an increase in the long wavelength absorbance. Thus, it appears that the formation of the product is decreased slightly by the formation of the new species. The possible nature of this species is discussed below.

The appearance of the new chromophoric species was not observed when the reaction was conducted at pH 6.0. Consequently, the O_2 concentration dependence could be evaluated over a larger range. Again, no concentration dependence was observed for any phase (data not shown).

The observed lack of O_2 concentration dependence for all of the phases of a reaction that requires O_2 to occur shows that a step prior to the observed steps is irreversible. It also suggests that the true O_2 binding step occurs in the dead time of the stopped-flow apparatus. An overlay of the spectra of the static anaerobic E−4NC complex with that recorded at 3.8 ms after addition of O_2 to the preformed complex (fastest phase being <1% complete) revealed that there are only minor changes associated with the initial oxygenated complex. Likewise, the first several spectra of the time course shown in Figure 6A show that small changes occur in the spectrum without formation of the product that would be revealed by a band at 330 nm. These observations suggest that the first two intermediates of the O_2 binding and reaction process [E−4NC−O_2(1) and E−4NC−O_2(2)], which maximize and decay within this time frame, spectroscopically resemble 4NC dianion, and thus, the aromatic ring of 4NC is intact. The large shift in the optical spectrum to that of the product occurs in the next part of the reaction time course during which the E−4NC−O_2(3) intermediate is formed, suggesting that this is the ring cleaving step. Accordingly, rapid chemical quench experiments show that <5, ~80, and 100% of the expected product is formed in the active site or released into solution after 0.5, 4, and 10 s, respectively, at 4 °C. These values are most consistent with product formation occurring with the 0.31 s^{-1} rate constant associated with E−4NC−O_2(3) formation before the overall rate-limiting product release in the final slow step (0.07 s^{-1}). Scheme 4 is the simplest model that can account for the observations. It is assumed that the species absorbing

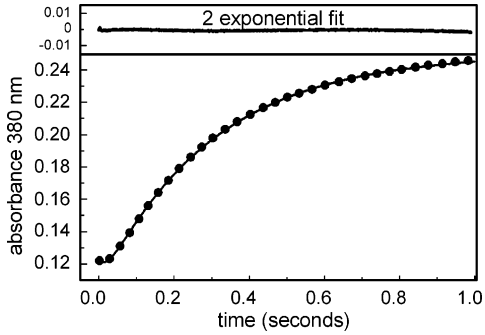

FIGURE 8: Single-wavelength time course of the reaction of the preformed 2,3-HPCD−HPCA complex with O_2. A premixed stoichiometric solution of 2,3-HPCD and HPCD (50 μM in the final reaction) was rapidly mixed using a stopped-flow device with O_2-enriched buffer (210 μM after mixing). The progress curve (•••) was fit to a summed two-exponential process (—). The residuals are shown at the top of the figure. Conditions: 50 mM MOPS, pH 7.5, and 4 °C.

between 425 and 625 nm in Figure 7 (designated EI) arises from a bifurcation of the reaction pathway at the product forming stage.

In contrast to the 4NC binding reaction, it is unlikely that the three observed phases of the E−4NC(3) reaction with O_2 are caused by different forms of the enzyme reacting in parallel for three reasons. First, the spectra of the first two intermediates, E−4NC−O_2(1) and E−4NC−O_2(2), suggest that the ring open product has not been formed. Second, a discrete phase associated with product forming reaction has been identified. Third, the correlation of the reciprocal relaxation time of the slowest phase with the turnover number shows that all of the enzyme must pass through the slowest-forming intermediate, presumably the enzyme−product complex.

Single Turnover of the Preformed E−HPCA Complex. For comparison, the reaction of the stoichiometric E−HPCA complex with O_2 was monitored at 380 nm where the natural product has a maximum absorbance. Although the precise K_d value for the E−HPCA complex is not known due to the lack of a spectral change as it forms, the value is lower than that for 4NC because HPCA displaces >80% of the 4NC from the complex when both the substrate and enzyme are present at 50 μM (data not shown). Moreover, HPCA and 4NC elicit similar K_m values for steady-state turnover as shown in Table 1. Thus, it is likely that a stoichiometric complex is formed upon anaerobic premixing at the concentrations that have been used. As shown in Figure 8, the time course exhibits a lag indicative of a multistep reaction. The traces were best fit by two summed exponentials (Table 2) in which the first phase was assigned a small negative amplitude. The slower phase has a large positive amplitude at the wavelength of the ring-cleaved product. The reciprocal relaxation time of this phase is 3.2 ± 0.2 s^{-1}, which is equal to the steady-state turnover number at 4 °C. Thus, the rate constant derived from the reciprocal relaxation time of the slower phase is certainly that of the ring cleaving step of the reaction, but it may also encompass the product release step since only one phase is detected beyond the initial fast phase. Neither of the observed phases showed a dependence on O_2 concentration (data not shown).

Many of the reactions in the steps following oxygen addition are likely to be irreversible for both the HPCA and

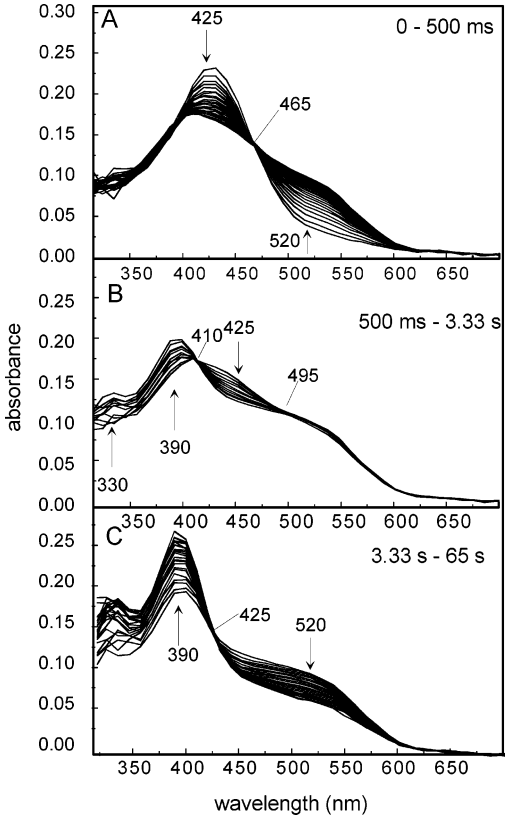

FIGURE 9: Rapid scan diode array spectra of the complete single-turnover reaction of 2,3-HPCD reacting with 4NC. Three time intervals of the same time course are shown. Arrows indicate the direction of change in absorbance, and lines indicate isosbestic points. 2,3-HPCD was rapidly mixed with 4NC in a stoichiometric ratio to a final concentration of 25 μM in air-saturated 50 mM MOPS at pH 7.5 and 4 °C.

4NC complexes due to the fact that they involve either O−O bond and aromatic ring cleavage or product release followed by spontaneous isomerization. Thus, the reciprocal relaxation times determined for the second half-reaction (Table 2) are probably good estimates of the forward rate constants of the later reaction steps.

Kinetics of the Complete Single-Turnover Cycle of 2,3-HPCD. Studies of the kinetics of the complete single-turnover reaction, in which both substrates were introduced to the enzyme at the same time, were conducted to determine whether the two half-reactions described thus far are fully descriptive of the complete reaction. 2,3-HPCD was rapidly mixed with a stoichiometric concentration of 4NC (vs active sites) at a concentration in large excess over the overall K_d in air-saturated 50 mM MOPS (pH 7.5). The monoanionic form of 4NC in solution was observed to bind to the enzyme, undergo conversion in part to the dianionic form, and then pass through several spectrally distinct intermediates leading to product formation. Three time intervals of the diode array spectral data set of the complete single-turnover reaction are shown in Figure 9. The first segment of the reaction shows that the level of the monoanionic form of 4NC ($\lambda_{max} = 425$ nm) decreases with a concomitant increase in that of the dianionic form ($\lambda_{max} = 520$ nm), and a characteristic isosbestic point is seen near 465 nm. In the complete cycle, one does not observe a stage in which all of the enzyme is in the dianionic 4NC-bound state. Rather, in the second segment of the reaction, product starts to form as indicated

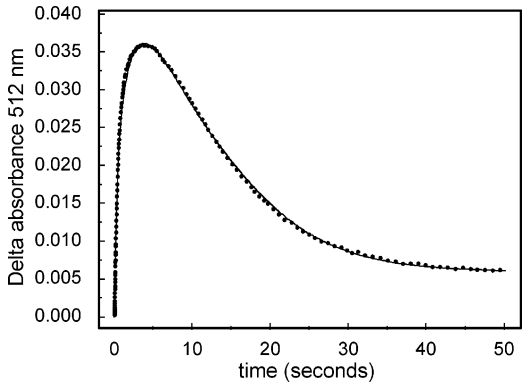

FIGURE 10: Single-wavelength time course of the complete single-turnover cycle of 2,3-HPCD with 4NC and O_2 at pH 7.5, recorded at 512 nm (•••) and a numerical integration simulation of the data (—) (see the Discussion). The data were simulated using the K_d value (325 μM) for the true first step in 4NC binding determined from the analysis of the kinetics (Figure 3) and rate constants obtained in the two half-reactions (see Schemes 3B and 4). Extinction coefficients (mM^{-1} cm^{-1}) used in the simulation were 0.4 for 4NC, 0.4 for E−4NC(1), 0.4 for E′−4NC(1), 13 for E−4NC(2), 13.5 for E−4NC(3), 13.5 for E−4NC−O_2(1), 12.5 for E−4NC−O_2(2), 1.2 for E−4NC−O_2(3), 2.2 for EI, and 1.15 for P. Reaction conditions are described in the legend of Figure 9.

by the absorbance increase at 390 and 330 nm. The amount of bound dianionic 4NC remains approximately constant during this period, suggesting that the rates of formation and decay of this intermediate are similar. There is an isosbestic point at 410 nm as would be expected for direct conversion from the monoanionic 4NC to product (see Figure 1A). However, on the basis of the constant concentration of dianionic 4NC, it is more likely that this isosbestic point arises from balanced conversion of the monoanionic to the dianionic form and dianionic form to product. This leads to a net conversion of monoanionic 4NC to product with no apparent change in the concentration of the dianionic species and, hence, the apparent isosbestic point. In the third segment, the monoanionic form is depleted and the dianionic form decays to product with the characteristic isosbestic point at 425 nm.

The analysis of the formation of the anaerobic E−4NC complex described above indicates that the initial complex for at least a portion of the enzyme is rather weak (K_d = 325 μM). Consequently, even when the enzyme and 4NC are present at concentrations well in excess of the overall dissociation constant, the first step of the complete single-turnover cycle does not proceed under pseudo-first-order conditions, nor does a stoichiometric complex form in the dead time of the instrument. Thus, the early time course is not expected to be fit by summed exponential phases. However, the high rates of the first steps relative to the later steps make it likely that a stoichiometric complex forms before the product forming steps, and thus, slower exponential phases may give accurate rate constants for the slower steps in the reaction. For the single-wavelength time course shown in Figure 10, summed exponential fitting reveals slow phase reciprocal relaxation times of 0.31 and 0.07 s^{-1} as observed for the product-forming half-reaction of the cycle. Thus, the intermediates and at least some of the rate constants observed for each half of the single-turnover cycle are also observed in the complete cycle. This can be examined in more detail using time course simulations (see the Discussion).

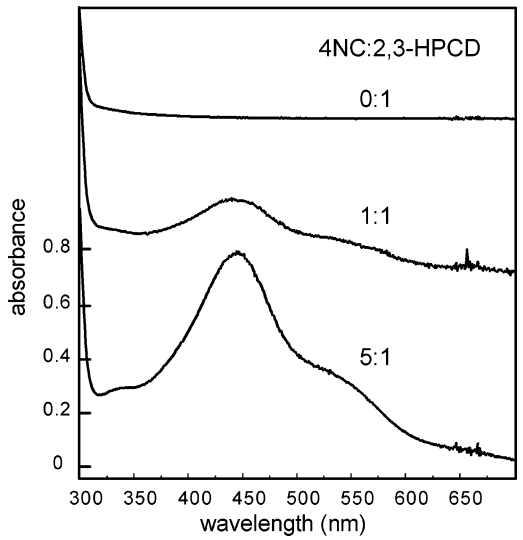

FIGURE 11: Optical spectra of 2,3-HPCD after turnover of 4NC at pH 7.5. 2,3-HPCD (120 μM, sites) was allowed to react with 4NC in the fold excess shown and then isolated from the product and unreacted substrate by ultrafiltration. The material giving rise to the chromophore remained tightly associated with the enzyme. The spectra are offset for clarity. The reaction was carried out at ambient temperature in 50 mM MOPS (pH 7.5) with a constant flow of O_2 in the headspace of a septum-stoppered reaction vial. EPR spectra of the same samples showed that the active site iron oxidizes at the same rate at which formation of the chromophore proceeds.

Postreaction Optical Spectra of 2,3-HPCD. As noted above, an unidentified product that absorbs in the 425−625 nm region forms during 2,3-HPCD turnover of 4NC. Separation of the normal ring cleavage product and unreacted 4NC was achieved by ultrafiltration, but the novel product remained tightly associated with the enzyme as shown in Figure 11. Concomitant with the appearance of this species, the Fe(II) center was oxidized to give an EPR spectrum characteristic of multiple Fe(III) $S = {}^5/_2$ species, as we have previously reported (*5*). After approximately three turnovers, the iron became completely oxidized, and the enzyme was found to be inactive. It seems likely that the chromophoric species is the dead-end complex of 4NC with the Fe(III) active site after oxidative inactivation during turnover. Indeed, addition of 4 N NaOH to the isolated enzyme sample followed by ultrafiltration to remove the precipitated enzyme resulted in an optical spectrum indistinguishable from that of the dianionic form of 4NC. Moreover, the spectrum of an Fe(III)−4NC model complex in a pH 7.5 solution shows a λ_{max} at 435 nm with shoulders at 330 and 530 nm reminiscent of that observed here for the inactive enzyme complex (*30*). Attempts to restore the activity of the dead-end enzyme complex by reduction were not successful, perhaps because the low potential of the complex results in rapid reoxidation by O_2.

pH Effects on Reaction Cycle Kinetics. It was noted above that the relative phase amplitudes change for the 4NC binding half-reaction with changes in pH. The overall effects of pH on the complete reaction are complex and will be described elsewhere. However, it is clear that ionization of 4NC and the protein both influence the rate. In addition, the rate constant for inactivation during 4NC turnover increases as the pH increases, further complicating determination of the true pH dependence. We have found in preliminary studies that each of the reciprocal relaxation times for substrate

binding increases with an increase in pH. The overall binding reaction appears to occur much faster at high pH because the amplitude for the fast first phase becomes much greater than those of the other slower phases. In contrast, the reciprocal relaxation times for the O_2 binding, product formation, and product release half of the reaction either are insensitive to pH ($1/\tau_1$ and $1/\tau_2$) or decrease with an increase in pH ($1/\tau_3$). The overall rate of the complete reaction determined from steady-state measurements decreases with an increase in pH in accord with the proposal that $1/\tau_3$ represents the rate-limiting product release process.

DISCUSSION

The transient kinetics of the extradiol dioxygenase reaction cycle have been difficult to examine in the past because the active site metal center does not provide convenient spectroscopic probes. Here, a different approach is taken by using the chromophoric features associated with the alternative substrate 4NC and the product of HPCA oxidation to monitor the reaction. Using this approach, intermediates have been detected for the first time in an extradiol dioxygenase reaction. The work presented here establishes a new protocol for the study of this important enzyme class, and it allows the first correlation of the proposed mechanism of catalysis with the intermediates that actually occur during the reaction cycle. This new approach and its significance to the extradiol dioxygenase mechanism are discussed here.

Steps in the Binding of 4NC to 2,3-HPCD. The results show that the binding reaction of 4NC to 2,3-HPCD occurs in three observable steps in addition to an unobserved initial rapid association step. The data analysis presented in the Results supports a scheme in which two forms of the resting enzyme react with 4NC in parallel steps before converging on a common set of intermediates (Scheme 3B). One form binds 4NC relatively weakly, but it allows rapid conversion to the dianionic form, pulling the reaction forward. In contrast, the second form has a high affinity for 4NC, but it promotes a much slower conversion to the dianion, serving to extend the binding reaction beyond 10 s at 4 °C. We have found no direct evidence for the presence of more than one structurally distinct protein form of 2,3-HPCD; SDS−PAGE gel and electrospray mass spectral analysis reveal only one polypeptide. However, multiple forms of a single protein are possible. For example, the X-ray crystal structures show that the enzyme has both open and closed conformations, and joint consideration of X-ray crystallographic and spectroscopic studies suggests that the iron can be either five- or six-coordinate (*10*, *16*). These results support another scenario in which the ionization state of the solvent ligands and/or active site residues may result in enzyme states that react differently with substrate during the deprotonation and binding process. It is unclear why the forms do not equilibrate to allow the high-affinity 4NC complex to rapidly convert to the low-affinity form, and thereby allow efficient 4NC dianion formation in the entire enzyme population. However, substrate binding in the active site of the high-affinity form may block the rapid interconversion if access to bulk solvent is denied.

It is also possible that the distribution of ionization states of the 4NC itself in solution is responsible for the pH-dependent phase amplitudes. However, this seems unlikely because 4NC is 85% ionized at pH 7.5. It becomes essentially 100% ionized at pH 8.8, but the change in the relative amplitude of the first and third phases shown in Figure 5 is 7-fold.

Scheme 5: Hypothesis for the Role of Metal-Bound Solvents in 4NC Binding

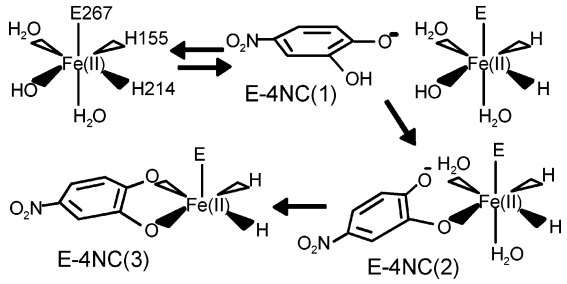

In related studies, we have mutated several potential active site bases.[2] The mutants vary widely in activity, but the kinetics of the substrate binding reaction are largely unchanged from those described here. Considered together, these results suggest that the pH-dependent changes cannot be attributed to either ionization of 4NC or an active site amino acid side chain. Thus, it is most likely that solvent ligand ionization is the major contributor.

The results show that 4NC remains in the monoanionic state in the rapidly formed initial complexes. This suggests that 4NC either does not bind to the iron in this complex or binds to the iron without changing its ionization state. During the longer time frame defined by the first and third observable exponential phases, the dianionic 4NC clearly forms. This involves deprotonation of the 4NC C3-OH group in the active site because the inductive effects of the NO_2 group cause the first deprotonation of 4NC in solution to occur at the C4-OH group. Deprotonation of the 4NC C3-OH group would seem to be a likely role for a putative anionic solvent ligand displaced from the iron during the binding process.

A Model for the Substrate Binding Process. One binding scenario that would account for the results is illustrated in Scheme 5. This hypothesis is based on the observation that the X-ray crystal structure shows that HPCA binds as an asymmetric chelate to the iron with the stronger bond formed by the C3 oxygen (see Scheme 1). Our spectroscopic studies of 2,3-CTD (*14*) and recent UV-resonance Raman studies of DHBD (*17*) show that the natural extradiol dioxygenase substrates bind as monoanionic chelates with the ionized hydroxyl group nearest the site of ring cleavage. The iron in the resting enzyme has three solvent ligands that are displaced as substrate binds. One of these solvents is likely to be hydroxide at the optimal reaction pH to establish a neutral Fe(II) center (the other charged ligand is a Glu267) as observed for other ring-cleaving dioxygenases (*18*, *35*). The hydroxide ligand may act as a convenient active site base as it is displaced to deprotonate the incoming C3 hydroxyl group of the neutral substrate to allow formation of an initial monodentate, monoanionic substrate complex with the iron that maintains the starting neutral state of the metal center. If 4NC binds in the same way as HPCA, as suggested by the conserved ring cleavage position, depro-

[2] S. L. Groce and J. D. Lipscomb, manuscript in preparation.

tonation of the 4NC C3-OH group would create the dianion rather than the monoanion, thereby accounting for the observed spectroscopic change. The formation of a substrate chelate requires displacement of a second solvent molecule. This may be a relatively slow process, especially in the case of 4NC because binding the deprotonated C4 hydroxyl to the iron would create a net charge on the initially neutral metal center. Presumably, the enzyme is not structured to neutralize this buried charge since it would not occur in the natural reaction cycle. The loss of the final water from the iron coordination may occur fairly rapidly once the substrate chelate has formed because it would allow the excess charge density to be partially dissipated (*16*).

The ability of ring-cleaving dioxygenases as a general class to optimize the binding rate of substrates (and ligand exchange in general) appears to be an important part of catalysis (*18*, *27*). For example, we and others have shown that the reactions of intradiol ring-cleaving dioxygenases also occur in multiple-substrate binding and product formation and release steps (*24*−*27*). In each step, the net charge of the metal center is maintained by exchanging anionic ligands just as we propose here for the extradiol class. When this process is disrupted by either mutagenesis or the use of substrates that assume a charge different from that of the natural substrate, the interconversion of intermediates becomes slow. In this case, this allows intermediates in the 4NC binding process to be detected easily using stopped-flow approaches.

The net charge of the iron center may provide an explanation for why the slowest phase of substrate binding dominates at low pH and nearly disappears at high pH. If all of the solvent ligands are protonated at low pH, then the Fe(II) site begins with a net charge of +1. The solvent cannot act as an effective base to deprotonate the incoming 4NC, slowing the reaction.

Steps in the O_2 Reaction with the 2,3-HPCD−*Substrate Complex.* The reaction of the preformed 2,3-HPCD−4NC complex with O_2 to form product shows three oxygen-independent kinetic phases at pH 7.5, suggesting that the reaction involves an unobserved, nearly irreversible, binding step followed by three additional steps (Scheme 4). Neither the intermediate formed in the stopped-flow dead time nor the following intermediate has spectral properties of the ring open product, so these represent steps in the reaction cycle preceding that critical step. It is reasonable that the unobserved first step involves O_2 binding to the iron since an open site adjacent to the iron is seen in the X-ray crystal structure (Scheme 1). The first observed step may then be a reorganization that perturbs the environment of the bound substrate.

The next intermediate exhibits the wavelength maxima expected for the product semialdehyde; thus, this appears to be the step in which ring cleavage occurs as indicated by the direct determination of the rate of product formation in the active site using chemical quench techniques. The final slow step results in a species that is spectrally indistinguishable from the ring cleavage product after isolation from the enzyme. Thus, the final step is probably product release, consistent with the finding that the rate of this step correlates with the turnover number. The true substrate of the enzyme, HPCA, appears to pass through a similar set of steps.

Scheme 6: Model for the Intermediates in the Complete Single-Turnover Reaction of 2,3-HPCD with 4NC

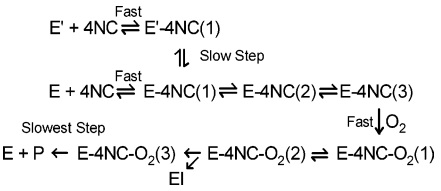

There is no evidence from the diode array spectra or the single-wavelength time course of the reaction of the preformed 2,3-HPCD−4NC complex with O_2 for conversion of dianionic 4NC to the monoanionic state prior to product formation. The most straightforward explanation for this is that the dianionic state is the reactive form of 4NC for this enzyme. These data do not rule out the possibility that the monoanionic state is also reactive, but this is made less likely by the analysis of the full single-turnover system described below.

Complete Single-Turnover Cycle. For the reasons stated in the Results, the complete single-turnover cycle cannot readily be set up such that the entire time course is described by summed exponential phases. However, the reaction time course can be simulated using numerical integration techniques by first assuming a mechanism, and then estimating the rate constants for each step and the extinction coefficients for each of the intermediates, substrate, and product. In the current case, the simplest way to proceed is to assume that the two half-reactions illustrated in Schemes 3B and 4 occur in sequence as illustrated in Scheme 6; the two half-reactions are connected by O_2 binding to the last species in the substrate binding process. With these assumptions, the current studies provide approximate rate constants for each step except for the rapid initial binding reactions of 4NC and O_2. These rate constants appear to be much larger than the others in the cycle, so as long as the forward constant is selected to be rapid relative to those of the ensuing steps, the specific values that are chosen will not affect the results. Once a forward rate constant for substrate binding is chosen, the K_d value (for the true first step at 4 °C) determined here establishes the reverse rate constant for the weakly associating enzyme fraction. The extinction coefficients for many of the species either are set by static spectra [substrate, product, E−4NC(3)] or can be approximated by amplitude or singular-value decomposition analysis of the half-reactions. It is found that the complex time course for the complete single-turnover reaction can be fit with the same mechanism, rate constants, and extinction coefficients determined in the nonlinear fits of the half-reactions. The fit for the time course monitored at 512 nm is shown superimposed on the data in Figure 10.

The model shown in Scheme 6 suggests that O_2 reacts with the final dianionic form of 4NC because if this were not the case, the very rapid initial reaction with O_2 seen in the product forming half-reaction would capture all of the enzyme before any of the dianionic 4NC could form. There is clearly substantial formation of the dianionic form during the reaction as seen in Figure 9. The small rate constant for the formation of the E−4NC(2) species from the E′−4NC(1) complex via the E−4NC(1) complex must also be included to give the somewhat protracted plateau region evident in the 512 nm trace of Figure 10 or in Figure 9B.

Scheme 7: Hypothesis for the Chemical Nature of the Intermediates that Occur during the Single-Turnover Cycle of 2,3-HPCD when 4NC Is Used as a Substrate

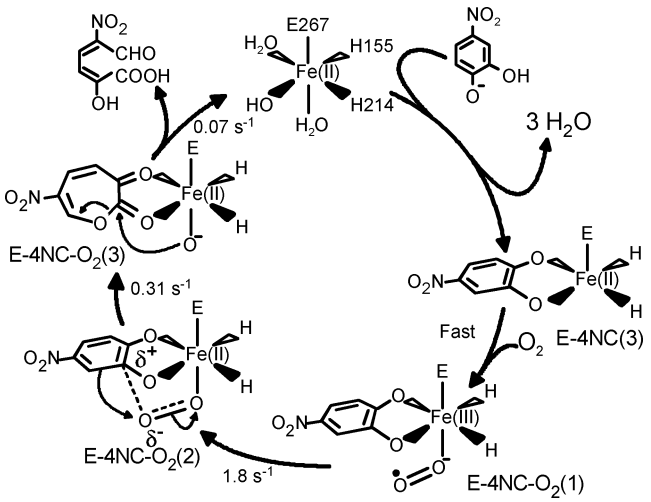

Similarly, the small rate constants for product formation and release determined from the half-reaction must be included in the simulation, showing that these occur at similar rates in the full turnover cycle. A chemical model for the intermediates in the complete turnover cycle is shown in Scheme 7.

The simulation was found to yield slightly too much product unless a branch at the E−4NC−O_2(2) species was included to allow some uncoupling of the reaction. This is in accord with the observed oxidation of the enzyme during turnover (see below).

Inactivation of 2,3-HPCD by 4NC. The results presented here and in our previous study (*5*) show that 2,3-HPCD is rapidly oxidized when turning over 4NC and that this occurs significantly more rapidly than during turnover of HPCA. The resulting Fe(III) site apparently readily binds 4NC as a dianion to give the enzyme a stable chromophore. Inactivation of extradiol dioxygenases during turnover of their natural substrates has been reported in many cases (*36*, *37*). Our laboratory has speculated that this is due to the loss of superoxide from an iron-bound superoxo intermediate before it attacks the substrate (*2*, *38*). This has been supported by detailed kinetic studies recently in the case of DHBD (*36*). It is also consistent with the model used here to simulate the full single-turnover cycle. The probability of losing superoxide would increase with the lifetime of the oxy intermediates shown in Scheme 7 [E−4NC−O_2(1) and E−4NC−O_2(2)]. This would depend on both the orientation of the substrate and its electronic character. The fact that intermediates form and decay much more slowly when 4NC is used in place of HPCA as the substrate suggests that the oxy intermediate may have a much longer lifetime. As a result, the inactivation reaction occurs in fewer turnovers.

Relationship of 4NC Turnover to Natural Substrate Turnover by Extradiol Dioxygenases. In past studies, it has been noted that 2,3-CTD appears to bind 4NC as the monoanion and has a much higher turnover number for this substrate than either the Mn(II) or Fe(II) form of homoprotocatechuate 2,3-dioxygenase (*30*, *31*). One interpretation of these results is that the monoanionic form of the substrate is required for efficient turnover, in accord with the observation that the natural substrates bind as monoanions. However, we have recently observed[2] that the K_i of 4NC for 2,3-CTD when it is used as an inhibitor (∼150 μM) is much higher than the reported K_m value (6.5 μM) when it is used as a substrate (*30*). When we combined 150 μM 2,3-CTD with a slight excess of 4NC, difference UV−vis spectroscopy showed substantial formation of the dianionic 4NC complex. Thus, we suspect that each of these extradiol dioxygenases binds 4NC as the dianion, and the higher rate in the case of 2,3-CTD follows from the fact that it is a more efficient enzyme for all substrates.

If the natural dioxygenase substrates bind in a different ionization state than 4NC, it is reasonable to ask whether this is at the root of the comparatively slow turnover of 4NC. On the basis of our proposal for the mechanism illustrated in Schemes 2 and 7, the monoanionic substrate passes through the dianionic state during the Criegee rearrangement [E−4NC−O_2(2) to E−4NC−O_2(3)]. Deprotonation provides one driving force for the rearrangement, and the proton derived from this ionization might be utilized to stabilize the anionic oxygen atom that results from O−O bond cleavage (*14*, *20*). When 4NC binds as the dianion prior to formation of an oxy complex, these methods of accelerating the reaction are lost. This may be an excellent example of the critical balance between metal Lewis acidity, substrate chemistry, and active site environment established in metalloenzymes to accelerate specific reactions.

It is interesting that despite the formation of a dianionic substrate, O_2 apparently does not attack the bound substrate directly as proposed for Fe(III)-containing intradiol dioxygenases (*2*, *3*). This may be due to two factors. First, the electron-withdrawing nitro group would deactivate electrophilic attack by O_2 as proposed for intradiol dioxygenases (*2*, *3*, *39*) while promoting the nucleophilic attack of bound nascent superoxide as proposed for the extradiol enzymes (*14*, *21*, *22*). Second, it is possible that the Fe(II) of the extradiol enzyme allows less delocalization of charge from the aromatic ring than the Fe(III) of the intradiol class. As a result, the aromatic ring has less radical character and the reaction with O_2 would be spin-forbidden. Since direct attack of O_2 appears to lead in nearly all cases to intradiol cleavage, prevention of the incorrect reaction regiospecificity may be an important role of Fe(II) in extradiol dioxygenases. The work described here provides the first methods for examining questions of this type at the level of reactions of specific intermediates in the reaction pathway of this important enzyme class.

ACKNOWLEDGMENT

We thank Dr. Beverly Ostrowski for assistance in obtaining the NMR spectrum of the 4NC product.

REFERENCES

1. Dagley, S. (1986) Biochemistry of aromatic hydrocarbon degradation in pseudomonads, in *The Bacteria* (Sokatch, J. R., Ed.) pp 527−556, Academic Press, New York.
2. Lipscomb, J. D., and Orville, A. M. (1992) Mechanistic aspects of dihydroxybenzoate dioxygenases, *Metal Ions Biol. Syst. 28*, 243−298.
3. Que, L., and Ho, R. Y. N. (1996) Dioxygen activation by enzymes with mononuclear non-heme iron active sites, *Chem. Rev. 96*, 2607−2624.

4. Vaillancourt, F. H., Bolin, J. T., and Eltis, L. D. (2003) Ring-cleavage dioxygenases, in *The Pseudomonads* (Ramos, J. L., Ed.) pp 359−395, Kluwer Academic/Plenum, New York.
5. Miller, M. A., and Lipscomb, J. D. (1996) Homoprotocatechuate 2,3-dioxygenase from *Brevibacterium fuscum*: a dioxygenase with catalase activity, *J. Biol. Chem. 271*, 5524−5535.
6. Whiting, A. K., Boldt, Y. R., Hendrich, M. P., Wackett, L. P., and Que, L., Jr. (1996) Manganese(ii)-dependent extradiol-cleaving catechol dioxygenase from *Arthrobacter globiformis* cm-2, *Biochemistry 35*, 160−170.
7. Kita, A., Kita, S., Fujisawa, I., Inaka, K., Ishida, T., Horiike, K., Nozaki, M., and Miki, K. (1999) An archetypical extradiol-cleaving catecholic dioxygenase: The crystal structure of catechol 2,3-dioxygenase (metapyrocatechase) from *Pseudomonas putida* mt-2, *Structure 7*, 25−34.
8. Senda, T., Sugiyama, K., Narita, H., Yamamoto, T., Kimbara, K., Fukuda, M., Sato, M., Yano, K., and Mitsui, Y. (1996) Three-dimensional structures of free form and two substrate complexes of an extradiol ring-cleavage type dioxygenase, the BphC enzyme from *Pseudomonas* sp. strain kks102, *J. Mol. Biol. 255*, 735−752.
9. Han, S., Eltis, L. D., Timmis, K. N., Muchmore, S. W., and Bolin, J. T. (1995) Crystal structure of the biphenyl-cleaving extradiol dioxygenase from a PCB-degrading pseudomonad, *Science 270*, 976−980.
10. Vetting, M. W., Wackett, L. P., Que, L., Jr., Lipscomb, J. D., and Ohlendorf, D. H. (2004) Crystallographic comparison of manganese- and iron-dependent homoprotocatechuate 2,3-dioxygenases, *J. Bacteriol. 186*, 1945−1958.
11. Hegg, E. L., and Que, L. (1997) The 2-His-1-carboxylate facial triad: An emerging structural motif in mononuclear non-heme iron(II) enzymes, *Eur. J. Biochem. 250*, 625−629.
12. Arciero, D. M., Lipscomb, J. D., Huynh, B. H., Kent, T. A., and Münck, E. (1983) EPR and Mössbauer studies of protocatechuate 4,5-dioxygenase. Characterization of a new Fe^{2+} environment, *J. Biol. Chem. 258*, 14981−14991.
13. Arciero, D. M., Orville, A. M., and Lipscomb, J. D. (1985) [^{17}O]-Water and nitric oxide binding by protocatechuate 4,5-dioxygenase and catechol 2,3-dioxygenase. Evidence for binding of exogenous ligands to the active site Fe^{2+} of extradiol dioxygenases, *J. Biol. Chem. 260*, 14035−14044.
14. Shu, L., Chiou, Y. M., Orville, A. M., Miller, M. A., Lipscomb, J. D., and Que, L., Jr. (1995) X-ray absorption spectroscopic studies of the Fe(II) active site of catechol 2,3-dioxygenase. Implications for the extradiol cleavage mechanism, *Biochemistry 34*, 6649−6659.
15. Mabrouk, P. A., Orville, A. M., Lipscomb, J. D., and Solomon, E. I. (1991) Variable-temperature variable-field magnetic circular dichroism studies of the iron(II) active site in metapyrocatechase: Implications for the molecular mechanism of extradiol dioxygenases, *J. Am. Chem. Soc. 113*, 4053−4061.
16. Davis, M. I., Wasinger, E. C., Decker, A., Pau, M. Y. M., Vaillancourt, F. H., Bolin, J. T., Eltis, L. D., Hedman, B., Hodgson, K. O., and Solomon, E. I. (2003) Spectroscopic and electronic structure studies of 2,3-dihydroxybiphenyl 1,2-dioxygenase: O_2 reactivity of the non-heme ferrous site in extradiol dioxygenases, *J. Am. Chem. Soc. 125*, 11214−11227.
17. Vaillancourt, F. H., Barbosa, C. J., Spiro, T. G., Bolin, J. T., Blades, M. W., Turner, R. F. B., and Eltis, L. D. (2002) Definitive evidence for monoanionic binding of 2,3-dihydroxybiphenyl to 2,3-dihydroxybiphenyl 1,2-dioxygenase from UV resonance Raman spectroscopy, UV/vis absorption spectroscopy, and crystallography, *J. Am. Chem. Soc. 124*, 2485−2496.
18. Orville, A. M., Lipscomb, J. D., and Ohlendorf, D. H. (1997) Crystal structures of substrate and substrate analog complexes of protocatechuate 3,4-dioxygenase: Endogenous Fe^{3+} ligand displacement in response to substrate binding, *Biochemistry 36*, 10052−10066.
19. Lee, S. K., and Lipscomb, J. D. (1999) Oxygen activation catalyzed by methane monooxygenase hydroxylase component: Proton delivery during the O−O bond cleavage steps, *Biochemistry 38*, 4423−4432.
20. Sato, N., Uragami, Y., Nishizaki, T., Takahashi, Y., Sazaki, G., Sugimoto, K., Nonaka, T., Masai, E., Fukuda, M., and Senda, T. (2002) Crystal structures of the reaction intermediate and its homologue of an extradiol-cleaving catecholic dioxygenase, *J. Mol. Biol. 321*, 621−636.
21. Arciero, D. M., and Lipscomb, J. D. (1986) Binding of ^{17}O-labeled substrate and inhibitors to protocatechuate 4,5-dioxygenase-nitrosyl complex. Evidence for direct substrate binding to the active site Fe^{2+} of extradiol dioxygenases, *J. Biol. Chem. 261*, 2170−2178.
22. Bugg, T. D. H. (2003) Dioxygenase enzymes: Catalytic mechanisms and chemical models, *Tetrahedron 59*, 7075−7101.
23. Criegee, R. (1948) The rearrangement of decahydronaphthalene peroxide esters resulting from cationic oxygen, *Annals 560*, 127−135.
24. Fujisawa, H., Hiromi, K., Uyeda, M., Okuno, S., and Nozaki, M. (1972) Protocatechuate 3,4-dioxygenase. 3. An oxygenated form of enzyme as reaction intermediate, *J. Biol. Chem. 247*, 4422−4428.
25. Whittaker, J. W., and Lipscomb, J. D. (1984) Transition state analogs for protocatechuate 3,4-dioxygenase. Spectroscopic and kinetic studies of the binding reactions of ketonized substrate analogs, *J. Biol. Chem. 259*, 4476−4486.
26. Bull, C., Ballou, D. P., and Otsuka, S. (1981) The reaction of oxygen with protocatechuate 3,4-dioxygenase from *Pseudomonas putida*. Characterization of a new oxygenated intermediate, *J. Biol. Chem. 256*, 12681−12686.
27. Frazee, R. W., Orville, A. M., Dolbeare, K. B., Yu, H., Ohlendorf, D. H., and Lipscomb, J. D. (1998) The axial tyrosinate Fe^{3+} ligand in protocatechuate 3,4-dioxygenase influences substrate binding and product release: Evidence for new reaction cycle intermediates, *Biochemistry 37*, 2131−2144.
28. Wolfe, M. D., Parales, J. V., Gibson, D. T., and Lipscomb, J. D. (2001) Single turnover chemistry and regulation of O_2 activation by the oxygenase component of naphthalene 1,2-dioxygenase, *J. Biol. Chem. 276*, 1945−1953.
29. Wolfe, M. D., Altier, D. J., Stubna, A., Popescu, C. V., Münck, E., and Lipscomb, J. D. (2002) Benzoate 1,2-dioxygenase from *Pseudomonas putida*: Single turnover kinetics and regulation of a two-component Rieske dioxygenase, *Biochemistry 41*, 9611−9626.
30. Tyson, C. A. (1975) 4-Nitrocatechol as a colorimetric probe for non-heme iron dioxygenases, *J. Biol. Chem. 250*, 1765−1770.
31. Reynolds, M. F., Costas, M., Ito, M., Jo, D.-H., Tipton, A. A., Whiting Adam, K., and Que, L., Jr. (2003) 4-Nitrocatechol as a probe of a Mn(II)-dependent extradiol-cleaving catechol dioxygenase (MndD): Comparison with relevant Fe(II) and Mn(II) model complexes, *J. Biol. Inorg. Chem. 8*, 263−272.
32. Whittaker, J. W., Orville, A. M., and Lipscomb, J. D. (1990) Protocatechuate 3,4-dioxygenase from *Brevibacterium fuscum*, *Methods Enzymol. 188*, 82−88.
33. Wang, Y. Z., and Lipscomb, J. D. (1997) Cloning, overexpression, and mutagenesis of the gene for homoprotocatechuate 2,3-dioxygenase from *Brevibacterium fuscum*, *Protein Expression Purif. 10*, 1−9.
34. Rosenblatt, D. H., Epstein, J., and Levitch, M. (1953) Some nuclearly substituted catechols and their acid dissociation constants, *J. Am. Chem. Soc. 75*, 3277−3278.
35. Orville, A. M., and Lipscomb, J. D. (1997) Cyanide and nitric oxide binding to reduced protocatechuate 3,4-dioxygenase: Insight into the basis for order-dependent ligand binding by intradiol catecholic dioxygenases, *Biochemistry 36*, 14044−14055.
36. Vaillancourt, F. H., Labbe, G., Drouin, N. M., Fortin, P. D., and Eltis, L. D. (2002) The mechanism-based inactivation of 2,3-dihydroxybiphenyl 1,2-dioxygenase by catecholic substrates, *J. Biol. Chem. 277*, 2019−2027.
37. Ono, K., Nozaki, M., and Hayaishi, O. (1970) Purification and some properties of protocatechuate 4,5-dioxygenase, *Biochim. Biophys. Acta 220*, 224−238.
38. Wolgel, S. A., Dege, J. E., Perkins-Olson, P. E., Jaurez-Garcia, C. H., Crawford, R. L., Münck, E., and Lipscomb, J. D. (1993) Purification and characterization of protocatechuate 2,3-dioxygenase from *Bacillus macerans*: A new extradiol catecholic dioxygenase, *J. Bacteriol. 175*, 4414−4426.
39. Que, L., Jr., Lipscomb, J. D., Münck, E., and Wood, J. M. (1977) Protocatechuate 3,4-dioxygenase. Inhibitor studies and mechanistic implications, *Biochim. Biophys. Acta 485*, 60−74.

BI048690X